Predictive gamma passing rate for three-dimensional dose verification with finite detector elements via improved dose uncertainty potential accumulation model

Eiji Shiba

Department of Radiation Oncology, Hospital of the University of Occupational and Environmental Health, Fukuoka 807-8556, Japan

Department of Radiation Oncology, Graduate School of Biomedical and Health Sciences, Hiroshima University, Hiroshima 734-8551, Japan

Akito Saito

Department of Radiation Oncology, Hiroshima University Hospital, Hiroshima 734-8551, Japan

Makoto Furumi

Department of Radiation Oncology, Hospital of the University of Occupational and Environmental Health, Fukuoka 807-8556, Japan

Daisuke Kawahara

Department of Radiation Oncology, Graduate School of Biomedical and Health Sciences, Hiroshima University, Hiroshima 734-8551, Japan

Kentaro Miki

Department of Radiation Oncology, Hiroshima University Hospital, Hiroshima 734-8551, Japan

Yuji Murakami

Department of Radiation Oncology, Graduate School of Biomedical and Health Sciences, Hiroshima University, Hiroshima 734-8551, Japan

Takayuki Ohguri

Department of Radiation Oncology, Hospital of the University of Occupational and Environmental Health, Fukuoka 807-8556, Japan

Shuichi Ozawa

Hiroshima High-Precision Radiotherapy Cancer Center, Hiroshima 732-0057, Japan

Department of Radiation Oncology, Graduate School of Biomedical and Health Sciences, Hiroshima University, Hiroshima 734-8551, Japan

Masato Tsuneda
Department of Radiation Oncology, Tokyo Women's Medical University, Shinjuku, Tokyo 162-8666, Japan

Katsuya Yahara
Department of Radiation Oncology, Hospital of the University of Occupational and Environmental Health, Fukuoka 807-8556, Japan

Teiji Nishio
Department of Medical Physics, Graduate School of Medical Science, Tokyo Women's Medical University, Tokyo 162-8666, Japan

Yukunori Korogi
Department of Radiation Oncology, Hospital of the University of Occupational and Environmental Health, Fukuoka 807-8556, Japan

Yasushi Nagata
Department of Radiation Oncology, Graduate School of Biomedical and Health Sciences, Hiroshima University, Hiroshima 734-8551, Japan

Corresponding author

Akito Saito, PhD
Department of Radiation Oncology, Hiroshima University Hospital
1-2-3 Kasumi, Minami, Hiroshima, Hiroshima 734-8551, Japan
Tel: +81-82-257-1545
Fax: +81-82-257-1546
E-mail: akito@hiroshima-u.ac.jp

Running title
Predictive 3D GPR via improved DUP model

Keywords

dose uncertainty
gamma passing rate
complexity metric

Abstract

Purpose: We aim to develop a method to predict the gamma passing rate (GPR) of a three-dimensional (3D) dose distribution measured by the Delta4 detector system using the dose uncertainty potential (DUP) accumulation model.
Methods: Sixty head-and-neck intensity-modulated radiation therapy (IMRT) treatment plans were created in the XiO treatment planning system. All plans were created using nine step-and-shoot beams of the ONCOR linear accelerator. Verification plans were created and measured by the Delta4 system. The planar DUP (pDUP) manifesting on a field edge was generated from the segmental aperture shape with a Gaussian folding on the beam's-eye view. The DUP at each voxel (u) was calculated by projecting the pDUP on the Delta4 phantom with its attenuation considered. The learning model (LM), an average GPR as a function of the DUP, was approximated by an exponential function $a\mathrm{GPR}(u) = e^{-qu}$ to compensate for the low statistics of the learning data due to a finite number of the detectors. The coefficient q was optimized to ensure that the difference between the measured and predicted GPRs (dGPR) was minimized. The standard deviation (SD) of the dGPR was evaluated for the optimized LM.
Results: It was confirmed that the coefficient q was larger for tighter tolerance. This result corresponds to the expectation that the attenuation of the $a\mathrm{GPR}(u)$ will be large for tighter tolerance. The pGPR and mGPR were observed to be proportional for all tolerances investigated. The SD of dGPR was 2.3, 4.1, and 6.7% for tolerances of 3%/3 mm, 3%/2 mm, 2%/2 mm, respectively.
Conclusion: The DUP-based predicting method of the GPR was extended to 3D by introducing DUP attenuation and an optimized analytical LM to compensate for the low statistics of the learning data due to a finite number of detector elements. The precision of the predicted GPR is expected to be improved by improving the LM and by involving other metrics.

1. Introduction

Intensity-modulated radiation therapy (IMRT) has become immensely popular in modern radiation therapy as it realizes a high dose conformality on the target volume. Since IMRT utilizes a complex intensity-modulation (IM) using a multileaf collimator (MLC) system, the patient-specific quality assurance (QA) has been emphasized as the pre-treatment verification. In practice, the patient-specific QA is typically performed using a pin-point ionization chamber for absolute dose verification and a two-dimensional (2D) or three-dimensional (3D) detector array to verify the shape of the dose distribution. Preparation for the patient-specific QA requires time and cost for the generation of the verification plan, measurements of the absolute dose and the dose distribution, and subsequent analysis with a certain occupation of the treatment machine. Thus, improving the efficiency of IMRT preparation is an essential concern to be addressed to meet the increasing demand for IMRT. Moreover, it is not feasible to use the IMRT for progressive diseases as the preparation of the IMRT takes longer than 3D conformal radiation therapy. Therefore, reducing the effort for IMRT preparation attracts attention in these contexts. In practice, the number of institutions performing the measurement-based patient-specific QA is dropping.[1] For example, the verification measurement for specific treatment sites such as the prostate or breast, in which a successful result is highly expected, has been reduced or stopped in some institutions. However, there is a need to develop a verification method that can substitute the currently used gamma analysis[2] without losing the safety level in the IMRT delivery.

Recently, a variety of attempts have been made to estimate the IM complexity and to investigate their relationship between the IM and gamma passing rate (GPR), which may potentially help to omit the patient-specific QA and to improve the efficiency of the clinical QA practice. A complexity metric (CM) that may be related to the GPR has been proposed by several authors,[3–10] resulting in limited predictability of the GPR. Deep learning (DL)-based prediction showed a good performance for the planar dose distribution measured using the film.[11] Recently, machine learning (ML) technique was used to attempt the GPR prediction using the CMs as input data.[12]

In our previous study, we developed a novel method to predict the GPR using a dose uncertainty potential (DUP) accumulation technique.[13] The concept of the DUP was first introduced by Kim et al.[14] Jin et al. further developed the concept[15, 16] and demonstrated its application to clinical data.[17] The essential result of our previous study[13] was that a good performance of the DUP-based prediction of the GPR was demonstrated for a planar dose distribution with a pixel size of 1×1 mm^2. This method is based on a hypothesis that the γ value depends on the DUP at each dose voxel. In this study, we aim to extend the application of our DUP-based method to 3D dose distribution analyzed using the gamma analysis with a finite number of detector elements. We introduced two techniques to apply our DUP-based method to the 3D data in this study. One is the DUP attenuation while estimating the 3D DUP distribution. Another is an optimized analytical learning model to compensate for the low statistics of the learning data due to a limited number of detectors in the device.

2. Materials and Methods

2.A. Clinical equipment, treatment plans, and patient-specific verification data

Figure 1 shows a schematic of the workflow. Sixty head-and-neck IMRT treatment plans were created in the XiO treatment planning system (TPS) (Elekta AB, Stockholm, Sweden). All plans were created using nine step-and-shoot beams of the ONCOR linear accelerator (Siemens Medical Systems, Concord, CA). The optimization was performed with the maximum iteration of 60 and the convergence criterion of 0.001%. The dose computation was performed with the grid spacing of 3 mm. Total number of segments in each plan is shown in Fig. 2(a) and the monitor unit (MU) of each segment is shown in Fig. 2(b). The minimum segmental MU among 60 plans was 2. The treatment plan and dose distribution were exported from the TPS in the digital imaging and communications in medicine (DICOM) format.

We used the Delta4 system that comprises of 1069 p-type Si semiconductors with an active area of 0.0078 cm^2. The phantom has a cylindrical shape with a 22-cm diameter and 40-cm length. The detector elements are arranged on two oblique planes at 50° and 320° on the axial view. The detectors are arranged in 20 × 20 cm^2 area on each plane. The detector spacing was 0.5 cm within the inner area of 6 × 6 cm^2 while 1 cm for the area outside of 6 × 6 cm^2.

Verification plans were created and measured by Delta4 (ScandiDos, Inc., Ashland, VA, USA).[18] The measured dose distribution (D_m) was compared with the calculated dose distribution (D_c) using the gamma analysis. The γ distribution was calculated from D_c and D_m on the detector elements on the oblique planes. The GPR was then calculated from the γ distribution and was exported to our in-house software (GPR analyzer).

The DICOM RT Plan was also used for generating the 3D DUP distribution using another in-house software (DUP generator) described in Sect. 2.B. The 3D DUP distribution was exported to the GPR analyzer which predicts the GPR. The GPR analyzer used the GPR from the Delta4 system and the 3D DUP distribution from the DUP generator to calculate the predicted GPR.

2.B. Generation of the three-dimensional distribution of dose uncertainty potential

A planar DUP (pDUP) distribution of each beam was generated using the same method developed in our previous study[13] using the segmental MLC shape and monitor unit extracted from the DICOM RT Plan. The width of the Gaussian folding was 3.9 mm as per the analysis of our previous study[13] but with the lateral profile of the 3 × 3-cm^2 MLC field at 11-cm depth with a source-to-surface distance (SSD) of 89 cm, which is the same as the center of the Delta4 device.

The attenuation of the DUP in the Delta4 phantom needs to be accounted for when the pDUP distribution is projected on the Delta4 phantom. The attenuation of the DUP was estimated using a dose distribution of a 3 × 3-cm^2 MLC field with the SSD = 89 cm. The dose distribution of the MLC field [Fig. 3(a)] was obtained, and the

differential of the dose distribution $u(d,x) = dD(d,x)/dx$ was calculated [Fig. 3(b)]. The depth profile of the DUP $U(d)$ is defined by

$$U(d) = \max\{u(d,x)\}\,\forall\{x\}. \quad (1)$$

Normalized depth profiles of $D(d,0)$ and $U(d)$ were created using

$$\widehat{D}(d) = D(d,0)/\max\{D(d,0)\}\,\forall\{d\} \text{ and} \quad (2)$$

$$\widehat{U}(d) = U(d)/\max\{U(d)\}\,\forall\{d\}. \quad (3)$$

Figure 3(c) shows $\widehat{D}(d)$ (solid line) and $\widehat{U}(d)$ (dashed line). Gray filled area shows the depth range in which the Delta4 detectors are located (d = 1–21 cm). The attenuation of $\widehat{D}(d)$ and $\widehat{U}(d)$ at the center of the Delta4 device (d = 11 cm; dotted line in Fig. 3(c)) were 0.474 and 0.519, respectively. The attenuation of $\widehat{U}$ is larger than $\widehat{D}$ by 9.5% (~ (0.519 – 0.474) / 0.474 × 100).

Figure 4 shows the flow of the generation of the 3D DUP distribution. The pDUP was projected on the Delta4 phantom by taking the divergence into account [Fig. 4(a)]. In this projection, the Gaussian folding width was assumed to be proportional to the source-to-voxel distance. The depth profile of the DUP was considered using Eq. (1). The projection was performed for all segments in all beams [Fig. 4(b)]. This calculation was performed with 1 × 1 × 1-mm^3 voxels. The DUP was quadratically accumulated using

$$\mathrm{DUP}_{i_\mathrm{V}}^2 = \sum_{i_\mathrm{B}} \sum_{i_\mathrm{S}} \left[U_{i_\mathrm{B},i_\mathrm{S}}\left(d_{i_\mathrm{B},i_\mathrm{V}}\right)\right]^2, \quad (4)$$

where i_B, i_S, and i_V are the identifiers of the beam, segment, and voxel, respectively, $d_{i_\mathrm{B},i_\mathrm{V}}$ is the depth of the i_V'th voxel for the i_B'th beam, $U_{i_\mathrm{B},i_\mathrm{S}}$ is the DUP for each set of $(i_\mathrm{B}, i_\mathrm{S}, i_\mathrm{V})$. The DUP values on the detector elements (oblique lines in Fig. 4(c)) were extracted and were used to predict the 3D GPR.

2.C. Prediction of gamma passing rate

Figure 5 shows a diagram of the GPR prediction. The learning data comprises of a set of the γ distribution [Fig. 5(a)] and DUP [u] distribution [Fig. 5(b)]. The γ distribution was translated to the measured GPR [mGPR] for the tolerance of 3%/3 mm, 3%/2 mm, and 2%/2 mm, which were obtained from the Delta4 software. The DUP histogram [$F_j(u)$, Fig. 5(c)] was obtained from the DUP distribution [Fig. 5(b)] (Step #1).

Our method is based on the hypothesis that the γ histogram depends on the DUP value. In our previous study, we demonstrated that this hypothesis is applicable for a planar dose distribution with 1 × 1-mm^2 pixel size.[13] One of the developments in this study is to apply our method to the gamma analysis using a fewer number of data points. Our previous study predicted the GPR using a full numerical data array of the γ and u distributions with 1 × 1-mm^2 pixels. The learning model (LM), an average GPR for a given DUP [aGPR(u)], was calculated from a large number of pixel data of γ and u values. On the other hand, this study predicts the GPR from the finite number of detector elements in Delta4. The LM was assumed to be an exponential function to avoid a statistical fluctuation due to the finite number of detectors [Fig. 5(d)].

The predicted GPR [pGPR] was calculated using the DUP histogram [Fig. 5(c)] and the LM [Fig. 5(d)]. The LM is defined as

$$a\mathrm{GPR}(u) = e^{-qu}, \tag{5}$$

where q is a parameter to optimize. The pGPR is calculated by

$$p\mathrm{GPR} = \sum_l \left[F_j(u_l) a\mathrm{GPR}(u_l)\right] / \sum_l F_j(u_l), \tag{6}$$

where j is the identifier of the learning data and l is the suffix for u. A squared sum of the difference between pGPR and mGPR for all data except for the evaluated data (i'th data) is calculated by

$$S_i = \sum_{j \neq i} d\mathrm{GPR}_j^2, \tag{7}$$

where

$$d\mathrm{GPR}_j = m\mathrm{GPR}_j - p\mathrm{GPR}_j \tag{8}$$

(Step #3). In practice, S_i depends on the parameter q, as illustrated in Fig. 5(e). Thus, the parameter q was optimized to give the minimum value of S_i. The optimized value of q [q_i^{opt}] was then used to determine the optimized LM [Fig. 5(f)] (Step #4). The optimized LM was applied to the evaluated data (i'th data).

The evaluated data comprised the same data set as the learning data: the γ distribution [Fig. 5(g)] and u distribution [Fig. 5(h)]. The u distribution was translated to the u histogram [Fig. 5(i)]. The pGPR of the i'th data was calculated using the same equation as Eq. (6), but with q_i^{opt} (Step #5). The $p\mathrm{GPR}_i$ was then compared with the $m\mathrm{GPR}_i$ from the Delta4 software [Fig. 5(j)]. The leave-one-out cross-validation was realized by excluding the evaluated data from the optimization of the LM. This procedure was performed for all sixty data with the 3%/3-mm, 3%/2-mm, and 2%/2-mm tolerances. The pGPR was evaluated in comparison with the mGPR. Standard deviation (SD) of the dGPR was calculated as a function of pGPR.

3. Results

Figure 6(a) shows an example of S_i as a function of q [Eq. (7)] for each tolerance. Red, blue, and green lines are data of the 3%/3-mm, 3%/2-mm, and 2%/2-mm tolerances. The filled circles show the minimum point for each tolerance. The q_i value to give the minimum value of S_i was the optimized q_i. Figure 6(b) shows the exponential functions corresponding to the optimized q_i for each tolerance. The larger value of q_i corresponds to the larger attenuation of the exponential function. Larger attenuation was observed for tighter tolerance.

The correlation between mGPR and pGPR is shown in Fig. 7(a). Red, blue, and green symbols show data for the 3%/3-mm, 3%/2-mm, and 2%/2-mm tolerances, respectively. This correlation is translated to the relationship between the dGPR and pGPR shown in Fig. 7(b). The SD of the dGPR for each pGPR domain with 5% pitch is shown in Fig. 7(c). The corresponding area of this SD is shown with a filled gray area in Fig. 7(b). Note that the SD for pGPR <85% was not calculated as the data had low statistics. Mean SD for the 3%/3-mm, 3%/2-mm, and 2%/2-mm tolerances were 2.3%, 4.1%, and 6.7%. The systematic error of the dGPR for the 3%/3-mm, 3%/2-mm, and 2%/2-mm tolerances were 0.05%, 0.1%, and 0.3%.

4. Discussion

The DUP-based prediction of the 3D GPR was realized by introducing two techniques. One is the behavior of the DUP in the Delta4 phantom. The width of the penumbra, which was involved as the Gaussian folding width previously, was also assumed to be proportional to the source-to-voxel distance. This width affects the depth profile of the DUP because the amplitude obtained in Eq. (1) depends on the width at each depth. Technically, the difference between $D(d,0)$ and $U(d)$ is due to the larger widths at larger depths. The depth profile of U should be correctly involved for estimating the 3D DUP distribution since the attenuation of U is larger than D. It should also be noted that the IM beam has several apertures with different shape and size, which may produce a different depth profile of each aperture. For simplicity, we assumed that the depth profile of the DUP is the same as the one for 3 × 3-cm^2 MLC field for all apertures.

The DUP was used in our model as the only metric for predicting the mGPR. Technically, the DUP, an accumulated dose gradient at each voxel, is expected to have a direct impact on the resulting dose accuracy. In practice, the decrease of the mGPR occurs due to a discrepancy between D_{calc} and D_{meas}. The performance of the DUP-based prediction of GPR is supported by the *ab initio* approach originally introduced by Kim et al.[14] and developed by Jin et al.[15–17] Though the current study showed a limited performance, our previous and current results demonstrated an efficacy of using DUP for predicting GPR. While we consider the DUP is a good candidate for the effective metric for GPR prediction, there are other candidates for the good metric for predicting GPR. For example, the dose discrepancy is observed for small MLC fields which are often used in IMRT. Though this study included the location and intensity of the DUP, the field size was not taken into account. The field size affects both the penumbra width and the depth profile of the DUP. Therefore, precision in predicting the GPR is expected to be improved by taking into account the aperture size in each segment.

A simple exponential function with a single parameter [Eq. (5)] was chosen as the LM in this study. It helps to restrict aGPR within the realistic range of 0–100%. The aGPR for u = 0 is fixed at 100% and decreases for larger u. The fact that q_i is larger for tighter tolerance is consistent with the expectation that the attenuation of aGPR is larger for tighter tolerance [Fig. 6(b)]. The approximation using the exponential function also helps to compensate for the low statistics of the sampling due to the finite number of detectors. It is expected that the prediction performance may be improved by adjusting the shape of the LM.

GPR prediction has been investigated by several authors in previous studies. These are roughly classified into two approaches. One is a complexity metric showing an average characteristic of the complexity of the IM beam. Total monitor unit,[5] the modulation complexity score developed by McNiven et al.,[3] total leaf travel[4] were investigated in comparison with the GPR. The other approach is a direct estimation of the GPR. Our DUP-based method,[13] the DL-based method,[11] and the ML-based method[12] are classified into this direct estimation. This approach utilizes some parameters which have characteristics of the IM beam and good proportionality to the GPR. Our previous and current studies can be used to understand the performance of the DUP for predicting the GPR.

One example is a comparison with the ML-based method. In this study, we obtained SD = 2.3% and 6.7% for the 3%/3 mm and 2%/2 mm tolerances, which are close to the ML-based methods which analyzed data of a helical

diode array with a 1-cm pitch and achieved SD = 2.1–2.4% and 5.4–5.8% for the 3%/3 mm and 2%/2 mm tolerances by involving 28 complexity metrics as input parameters.[12] We consider that the DUP is an effective metric for predicting GPR since the DUP-based method achieved current results only with the DUP. The performance of our method is expected to be improved by involving other parameters such as the field size.

Another example is a comparison with the DL-based method as an ultimate approach which automatically involves multiple characteristics. Tomori et al.[11] analyzed data of composite dose distributions measured using a gafchromic film and obtained a root mean square error of 1.11%, 1.50%, and 2.24% for the 3%/3 mm, 3%/2 mm, and 2%/2 mm tolerances, which were smaller than our results (2.3, 4.1, and 6.7%) by factor of 2, 3, and 3, respectively. Since our data were obtained from the Delta4 system with a 5-mm pitch detector array, direct comparisons of these results do not provide an exact goal to achieve. Applying multiple predicting methods (e.g. the DUP-based, ML-based, and DL-based methods) to the same data set of the GPR may provide useful insight to understand how dominant the DUP is within the metrics for GPR prediction.

The SD of dGPR was evaluated in this study as well as our previous study. While the performances of the GPR predictions in previous studies were evaluated using Pearson's correlation coefficient r, a careful consideration is needed to employ the r for inter-comparison of the performance of the GPR predictions. The range of mGPR may differ among different combinations of the TPS, linear accelerator, and QA device. The quality of the beam model directly affects the range of the resulting mGPR and subsequent r value. Thus, we employed the SD of dGPR in our current and previous studies.

The use of SD for evaluating pGPR is also useful for considering the clinical application of the GPR prediction. The decision to use a predicting method may be based on the accuracy and precision of pGPR. In our previous study, we introduced an example consideration for estimating a threshold for pGPR corresponding to $m\text{GPR} \geq 90\%$ for a given confidence level.[13] This technique may be useful for considering a clinical use of pGPR with good accuracy and precision. Since we obtained a limited performance in this study, the consideration for the clinical use was left for our future study.

Sixty head-and-neck IMRT cases were used to develop the 3D GPR prediction method in this study. The evaluation of the necessary number of the learning data is left for our future study since other improvements such as using correct aperture size instead of the fixed 3×3 cm^2 and involving the effect of the field size may have larger impact in our development of the GPR prediction. It is necessary to test this method for other treatment sites such as in the brain, thorax, abdomen, and pelvis. Since the complexity of the treatment plan differs among treatment sites, it is expected that the quality of the LM will depend on the treatment site. It should also be noted that the DUP distribution differs among different IM techniques (e.g., step and shoot vs. sliding window, flattening filter vs. flattening filter free, IMRT vs. VMAT). Specifically, the VMAT delivery involves continuous and dynamic motion of the gantry and MLC. It is necessary to examine the application of our technique to VMAT since we generate the composite DUP by accumulating segmental DUPs as static gantry angle and the MLC shape at each segment. Thus, the LM needs to be generated and examined for each IM technique. The DUP distribution also differs among different TPSs and the accompanying algorithm. Therefore, further investigations are needed to obtain a general understanding of the DUP and its application to the GPR prediction.

5. Conclusion

We developed and demonstrated a DUP-based method to predict the GPR of the 3D dose distribution measured by a commercial 3D detector array system. The pDUP was extended to 3D by including the depth profile of the DUP. An approximated LM was employed to compensate for the finite statistics of the learning data. It is expected that this method can provide the predicted GPR prior to the verification measurements of the IMRT delivery.

Acknowledgement

We would like to thank Editage (www.editage.jp) for English language editing.

Disclosure of Conflict of Interest

The authors have no conflicts to disclose.

References

[1] Abolaban F, Zaman S, Cashmore J, Nisbet A, Clark CH. Changes in patterns of intensity-modulated radiotherapy verification and quality assurance in the UK. *Clin Oncol.* 2016;28:e28–e34.

[2] Low DA, Harms WB, Mutic S, Purdy JA. A technique for the quantitative evaluation of dose distributions, *Med Phys.* 1998;25:656–661.

[3] McNiven AL, Sharpe MB, Purdie TG. A new metric for assessing IMRT modulation complexity and plan deliverability. *Med Phys.* 2010;37:505–515.

[4] Masi L, Doro R, Favuzza V, Cipressi S, Livi L. Impact of plan parameters on the dosimetric accuracy of volumetric modulated arc therapy. *Med Phys.* 2013;40:071718.

[5] Agnew CE, Irvine DM, McGarry CK. Correlation of phantom-based and log file patient-specific QA with complexity scores for VMAT. *J Appl Clin Med Phys.* 2014;15:204–216.

[6] Rajasekaran D, Jeevanandam P, Sukumar P, Ranganathan A, Johnjothi S, and Nagarajan V. A study on the correlation between plan complexity and gamma index analysis in patient specific quality assurance of volumetric modulated arc therapy. *Rep Pract Oncol Radiother.* 2015;20:57–65.

[7] Kosaka K, Tanooka M, Doi H, et al. Feasibility of estimating patient-specific dose verification results directly from linear accelerator log files in volumetric modulated arc therapy. *Int J Med Phys Clin Eng Radiat Oncol.* 2016;5:317–328.

[8] Götstedt J, Hauer AK, Bäck A. Development and evaluation of aperture-based complexity metrics using film and EPID measurements of static MLC openings. *Med Phys.* 2015;42:3911–3921.

[9] Wang J, Jin X, Peng J, Xie J, Chen J, Hu W. Are simple IMRT beams more robust against MLC error? Exploring the impact of MLC errors on planar quality assurance and plan quality for different complexity beams. *J Appl Clin Med Phys.* 2016;17:147–157.

[10] Sumida I, Yamaguchi H, Das IJ, et al. Organ-specific modulation complexity score for the evaluation of dose delivery. *J Radiat Res.* 2017;58:675–684.

[11] Tomori S, Kadoya N, Takayama Y, et al. A deep learning-based prediction model for gamma evaluation in patient-specific quality assurance. *Med Phys.* 2018;45:4055–4065.

[12] Ono T, Hirashima H, Iramina H, et al. Prediction of dosimetric accuracy for VMAT plans using plan complexity parameters via machine learning. *Med Phys.* 2019;46:3823–3832.

[13] Shiba E, Saito A, Furumi M, et al. Predictive gamma passing rate by dose uncertainty potential accumulation model. *Med Phys.* 2019;46:999–1005.

[14] Kim S, Jin H, Chung H, Palta J, Ye SJ. Potential uncertainty – information that was forgotten. In: Yi B Ahn S, Choi E, eds. Proc. XIVth Int'l Conf. on the Use of Computers in Radiation Therapy; 2004:139–141.

[15] Jin H, Chung H, Liu C, Palta J, Suh TS, Kim S. A novel dose uncertainty model and its application for dose verification. *Med Phys.* 2005;32:1747–1756.

[16] Jin H, Palta J, Suh TS, Kim S. A generalized a priori dose uncertainty model of IMRT delivery. *Med Phys.* 2008;35:982–996.

[17] Jin H, Palta JR, Kim YH, Kim S. Application of a novel dose-uncertainty model for dose-uncertainty analysis in prostate intensity-modulated radiotherapy. *Int J Radiat Oncol Biol Phys.* 2010;78:920–928.

[18] Geurts M, Gonzalez J, Serrano-Ojeda P. Longitudinal study using a diode phantom for helical tomotherapy IMRT QA. *Med Phys.* 2009;36:4977–4983.

Figure Legends

Fig. 1. The workflow of this study.

Fig. 2. (a) Total number of segments in each plan and (b) the monitor unit of each segment.

Fig. 3. (a) Dose distribution [$D(d,x)$] and (b) $dD(d,x)/dx$ of a 3 × 3-cm^2 MLC field. (c) Normalized depth profile of the dose along the central axis [$\widehat{D}(d)$] and the DUP [$\widehat{U}(d)$]. Gray area shows the range in which the Delta4 detectors are located (d = 1–21 cm).

Fig. 4. Generation of the 3D distribution of the DUP.

Fig. 5. Diagram of the prediction of the gamma passing rate.

Fig. 6. (a) An example of S_i as a function of q [Eq. (7)]. Filled circles show the minimum point for each tolerance. (b) Exponential functions corresponding to the q_i^{opt}. The red, blue, and green lines represent data for the 3%/3-mm, 3%/2-mm, and 2%/2-mm tolerances, respectively.

Fig. 7. (a) Correlation between the mGPR and pGPR. Red, blue, and green plots are data of the 3%/3-mm, 3%/2-mm, and 2%/2-mm tolerances, respectively. (b) Difference between mGPR and pGPR as a function of pGPR. A filled gray area shows the range of a standard deviation (SD) for each domain of pGPR. (c) SD of the dGPR as a function of pGPR.

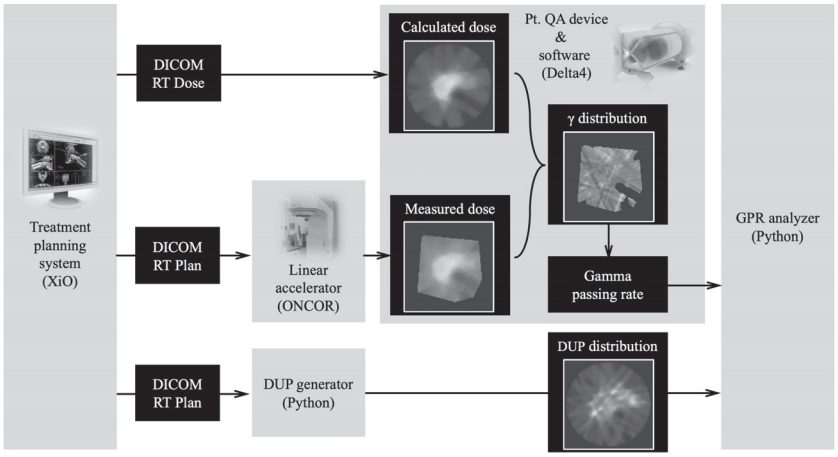

mp_13985_f1.tiff

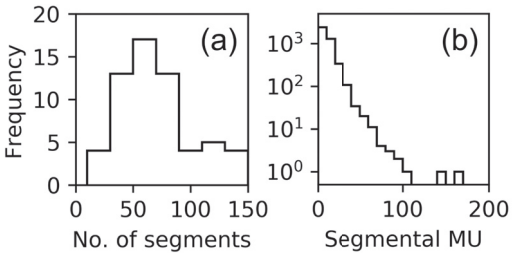

mp_13985_f2.tiff

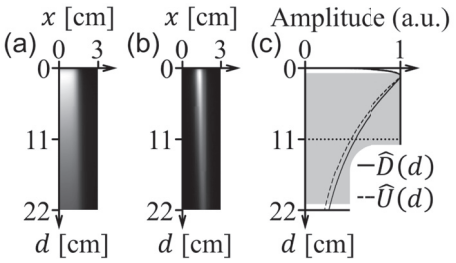

mp_13985_f3.tiff

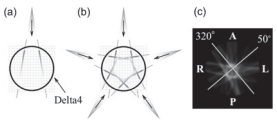

mp_13985_f4.tiff

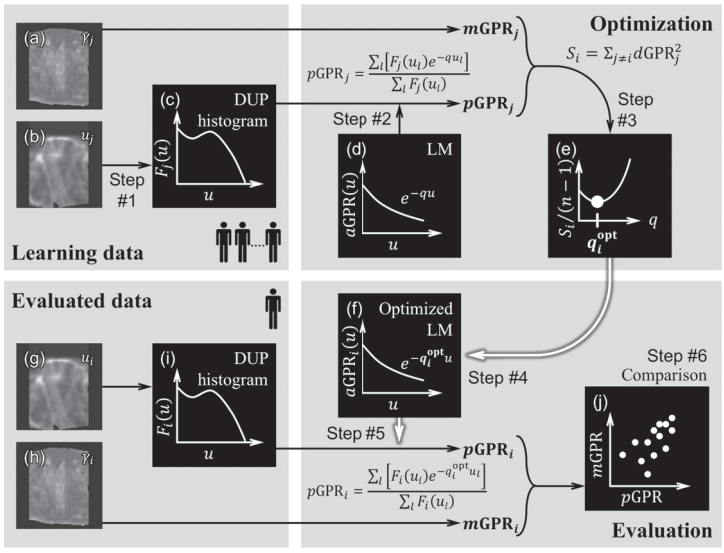

mp_13985_f5.tiff

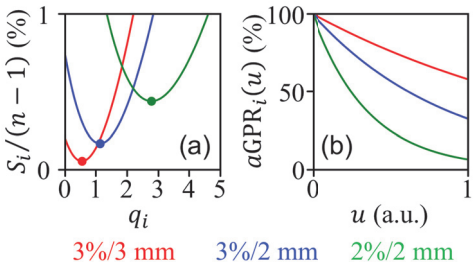

mp_13985_f6.tiff

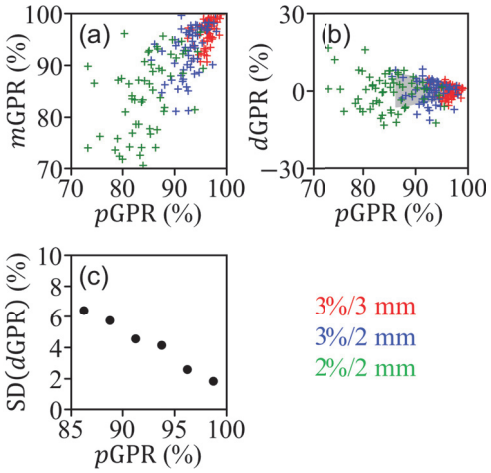

mp_13985_f7.tiff

It is not just a tagline. It is who we are, what we do and what makes us different. We have continually introduced important cancer treatment breakthroughs that help our customers improve outcomes for patients.

PATIENT-FIRST PRECISION
Confidently delivering effective treatments with minimal side effects.

PATIENT-FIRST VERSATILITY
Making personalized treatments practical for every patient.

PATIENT-FIRST EFFICIENCY
Ensuring fewer treatments and a faster return to daily life.

FIND OUT MORE ON THE NEW ACCURAY.COM/CONTACT-INQUIRY

#ACCURAYPATIENTFIRST

ACCURAY®

Important Safety Information

Most side effects of radiotherapy, including radiotherapy delivered with Accuray systems, are mild and temporary, often involving fatigue, nausea, and skin irritation. Side effects can be severe, however, leading to pain, alterations in normal body functions (for example, urinary or salivary function), deterioration of quality of life, permanent injury, and even death. Side effects can occur during or shortly after radiation treatment or in the months and years following radiation. The nature and severity of side effects depend on many factors, including the size and location of the treated tumor, the treatment technique (for example, the radiation dose), and the patient's general medical condition, to name a few. For more details about the side effects of your radiation therapy, and to see if treatment with an Accuray product is right for you, ask your doctor.

MKT-ARA-0118-0191